

## **Supporting Information for**

### **Highly Efficient and Stable Pure 2D Perovskite Based Solar Cells**

#### **with 3-Aminopropionitrile Organic Cation**

*Yaru Li, Yang Zhao, Haoliang Cheng, Ke Zhao and Zhong-Sheng Wang\**

Department of Chemistry, Shanghai Key Laboratory of Molecular Catalysis and Innovative Materials, Laboratory of Advanced Materials, iChEM (Collaborative Innovation Center of Chemistry for Energy Materials), Fudan University, 2205 Songhu Road, Shanghai 200438, China.

\* Corresponding author: [zs.wang@fudan.edu.cn](mailto:zs.wang@fudan.edu.cn)

## Experimental Section

### Materials

Lead iodide ( $\text{PbI}_2$ , 99.99%) and PCBM were purchased from Xi'an Polymer Light Technology Corp. N, N-Dimethylformamide (DMF, 99.8%). Chlorobenzene (CB, 99.5%), 3-aminopropionitrile (3-APN) (97%) and hydroiodic acid (HI, 57 wt. % in  $\text{H}_2\text{O}$ ) were purchased from J&K Scientific.  $\text{Ni}(\text{NO}_3)_2 \cdot 6\text{H}_2\text{O}$  (0.291 g) (98%), ethyleneglycol (98%) and ethylenediamine (EDA, 99%) were purchased from Sinopharm Chemical Reagent Co. Ltd. All reagents were used as received without further purification.

### Synthesis of 3-APNI

The solution of 3-APN (500 mg, 7.14 mmol) was suspended in ethanol (20 mL) in an ice-water bath, to which an HI solution was added dropwise (1.60 g). The reaction mixture was stirred at 0 °C for 4 h, and then the solvent was removed under reduced pressure. The resulting solid was further washed three times using diethyl ether and dried at 60° in a vacuum oven. Finally, the white product of 3-APNI was collected and characterized with  $^1\text{H}$  NMR and  $^{13}\text{C}$  NMR.  $^1\text{H}$  NMR (400 MHz,  $\text{DMSO-d}_6$ ,  $\delta$ ): 7.97 (s, 3 H), 3.10 (t,  $J=8.0$  Hz, 2 H), 2.83 (t,  $J=6.0$  Hz, 2 H).  $^{13}\text{C}$  NMR (100 MHz,  $\text{DMSO-d}_6$ ): 118.2, 35.4, 16.3.

### Device fabrication

The etched indium tin oxide (ITO, 10  $\Omega$  per square, transmittance 88%, Shenzhen Huayu United Technology Co., Ltd) conducting glasses were ultrasonically cleaned with detergent, deionized water, acetone, and isopropyl alcohol sequentially for 30 min each. Afterwards, the substrates were treated with UV-ozone for 15 min. The NiOx precursor solution was prepared by

mixing  $\text{Ni}(\text{NO}_3)_2 \cdot 6\text{H}_2\text{O}$  (0.291 g) and EDA (50  $\mu\text{L}$ ) in ethyleneglycol (1 mL), which was then spin-coated onto the pre-cleaned ITO substrates at 4000 rpm for 90 s followed by annealing at 300 °C for 60 min. The substrates were then transferred into the glove box and pre-heated for 5 min before the deposition of active layer. The  $(3\text{-APN})_2\text{PbI}_4$  perovskite precursor solution was prepared in a stoichiometric ratio of 2:1 of 3-APNI and  $\text{PbI}_2$  in DMF solvent, in which the concentration of  $\text{Pb}^{2+}$  is 0.3 M. The solution was stirred at 70 °C for 6 h before use. 60  $\mu\text{L}$  of the prepared perovskite precursor solution was spin-coated at 5000 rpm for 30 s onto the ITO/NiOx substrate and annealed at 100 °C for 10 min. After deposition of the perovskite active layer, the PCBM solution was spin-coated on top of the perovskite films at 1600 rpm for 30 s. Finally, the films were transferred to a vacuum chamber, and 100 nm thick Ag electrode was deposited on the PCBM film. The device area is defined to be 0.10  $\text{cm}^2$  with a metal mask.

### **Characterization**

X-ray diffraction (XRD) pattern was measured by Bruker D8 Advance X-ray diffractometer (Cu  $\text{K}\alpha 1$ ,  $\lambda = 0.154$  nm; 40 kV, 40 mA). Film morphology was obtained with a field emission scanning electron microscope (FE-SEM-4800-1) and an atomic force microscopy (NANO4). Steady-state photoluminescence (PL) spectra were measured using a spectrofluorophotometer (RF-5301PC, Shimadzu) with a monochromatic light (520 nm) from a xenon lamp source. Ultraviolet photoelectron spectroscopy (UPS) measurements are carried out using a Kratos AXIS ULTRA DALD XPS/UPS system. The UPS measurements are conducted by Shimadzu Spectrometer (AXIS ULTRA DLD) with a He I (21.2 eV) discharge lamp. The current density-voltage ( $J$ - $V$ ) characteristics of the devices were measured at 100  $\text{mW cm}^{-2}$  AM1.5G illumination with a computer-controlled Keithley 2420 source meter and Newport-94043A solar simulator (300 W). The incident photon-to-electron conversion efficiency (IPCE) spectra were recorded on

a SM-250 hyper mono-light system (Bunkoukeiki, Japan). High-resolution transmission electron microscopy (HRTEM) images were obtained from JEM-2100F. Grazing-Incidence Wide-Angle X-ray Scattering (GIWAXS) measurements were performed at the MetalJet-D2 Excillum X-ray source (Xenocs-SAXS/WAXS, France) with a wavelength of 1.54189 Å and the samples were treated at an incident angle of 0.2°. The scattering signal was collected by a Pilatus 200 K detector and placed 198.84 mm away from the sample position. The apparent hole/electron mobility ( $\mu$ ) was calculated with the Mott-Gurney law, given by the equation of  $J = 9\epsilon_0\epsilon_r\mu V^2/(8L^3)$ , where  $J$  stands for the current density,  $\epsilon_0$  is the permittivity of free space,  $\epsilon_r$  is the relative permittivity of the medium,  $\mu$  is the mobility of hole or electron,  $V$  is the effective voltage, and  $L$  is the thickness of the active layer. The hole and electron mobility can be calculated from the slope of the  $J^{0.5}$ - $V$  curve.

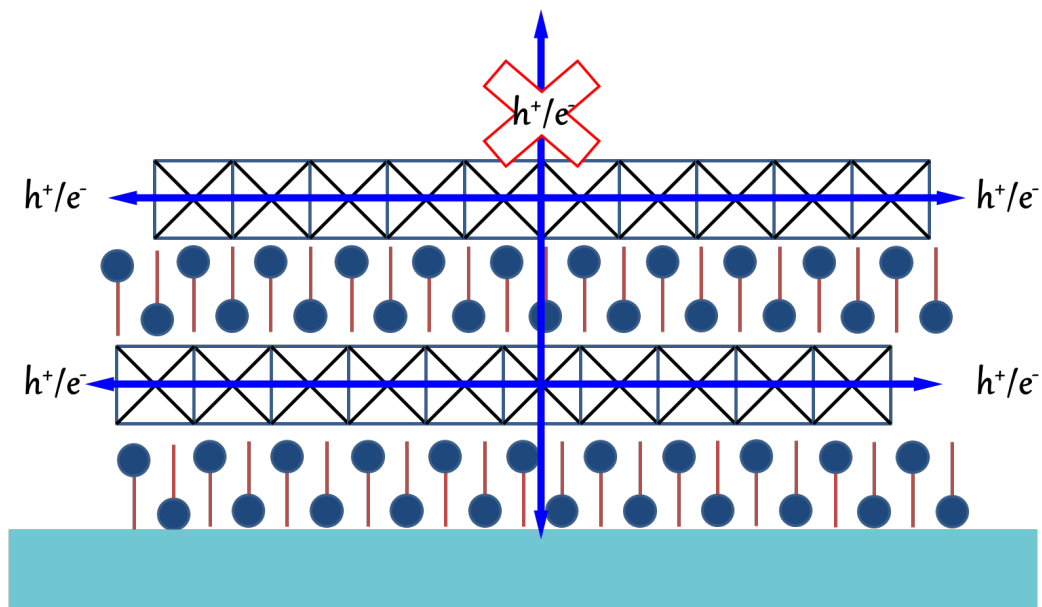


**Figure S1.** The diagrammatic sketch of the hole/electron ( $h^+/e^-$ ) transport in the pure 2D perovskite that grows in a regular parallel orientation to the substrate.

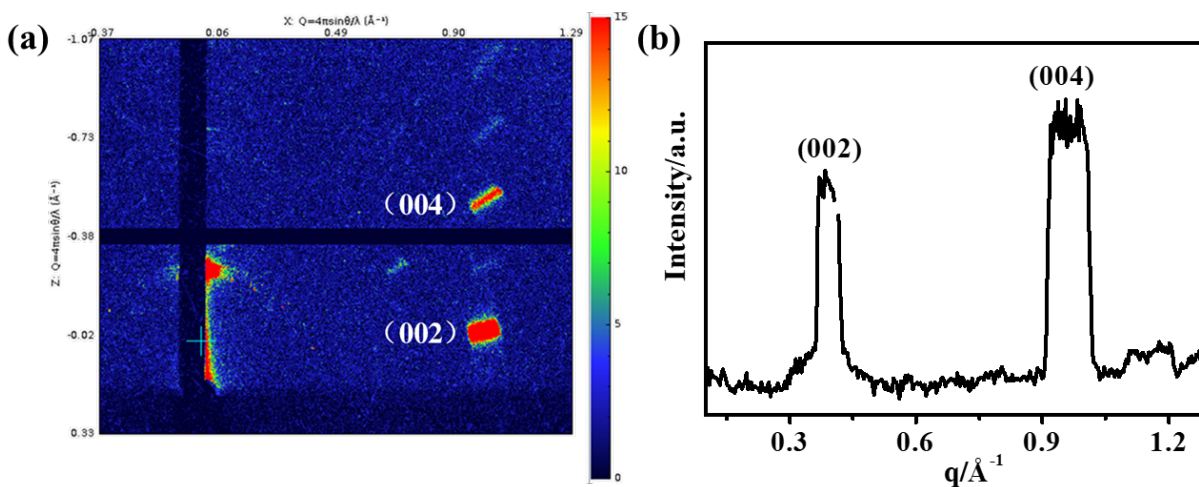


**Figure S2.** (a) The GIWAXS profiles and (b) the intensity versus  $q$  ( $q = 4\pi \sin \theta / \lambda$ ) for the diffraction features for the pure 2D  $\text{BA}_2\text{PbI}_4$  (BA = butylammonium).

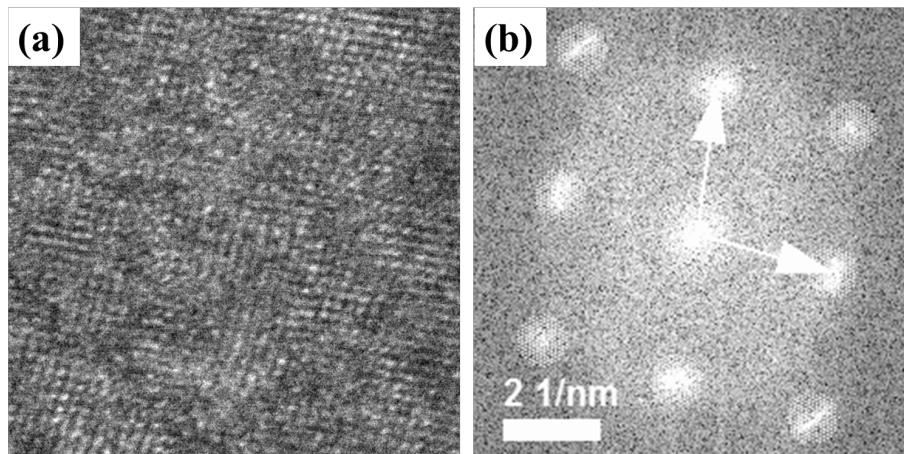


**Figure S3.** (a) HRTEM images and (b) the corresponding diffraction patterns after FFT process of  $(3\text{-APN})_2\text{PbI}_4$  perovskite film.

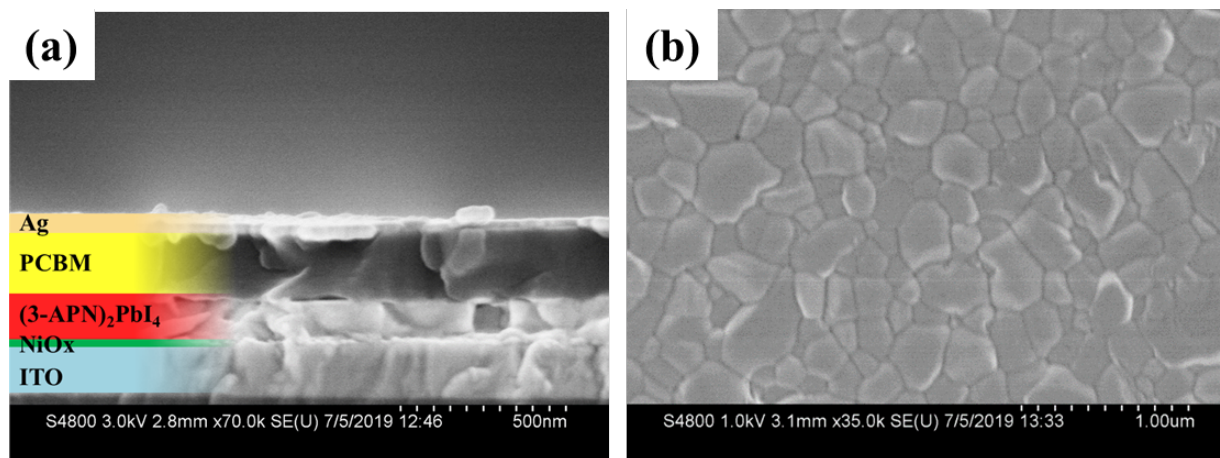


**Figure S4.** (a) The cross-sectional scanning electron microscope (SEM) image of the device. (b) The top-view SEM image of  $(3\text{-APN})_2\text{PbI}_4$  film.

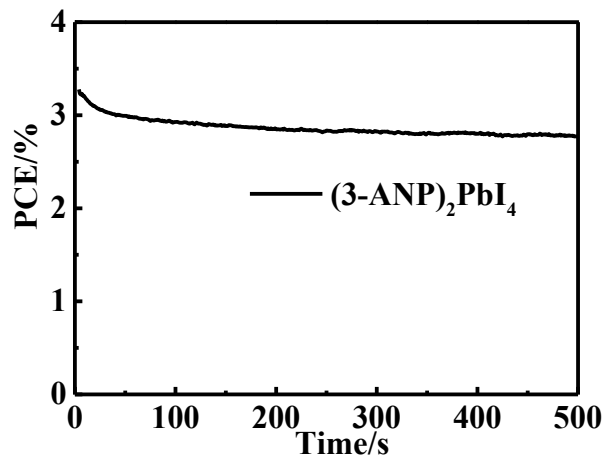


Figure S5. The stabilized power output of the champion device measured at a fixed maximum power point voltage as a function of time (25 °C, relative humidity of 45%).

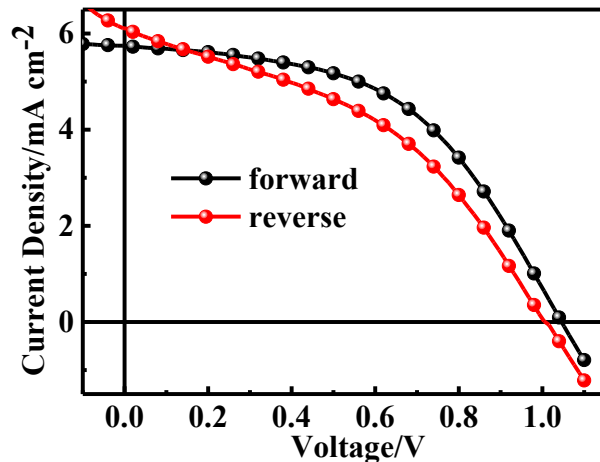


Figure S6.  $J$ - $V$  characteristics for the  $(3\text{-APN})_2\text{PbI}_4$  based PSC measured at forward and reverse scan directions.

Table S1. Photovoltaic performance parameters of the  $(3\text{-APN})_2\text{PbI}_4$  based PSC under forward and reverse scan directions

Scan direction	$V_{oc}/V$	$J_{sc}/\text{mA cm}^{-2}$	FF	PCE/%
Forward	1.05	5.74	0.50	3.01
Reverse	1.01	6.13	0.41	2.54

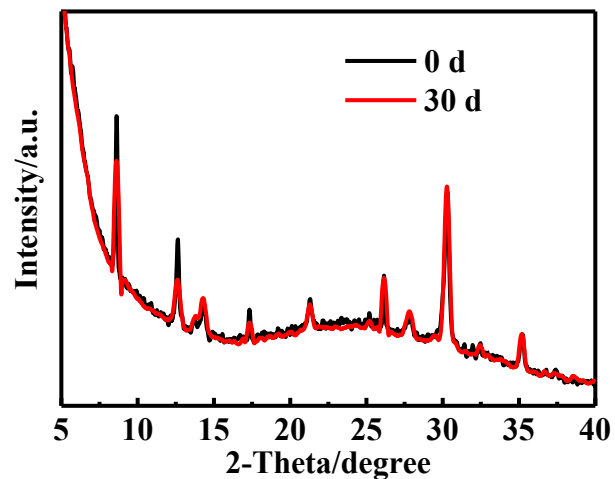


Figure S7. The XRD patterns of the  $(3\text{-APN})_2\text{PbI}_4$  film stored in air with 45% RH at room temperature for 0 day and 30 days, respectively.

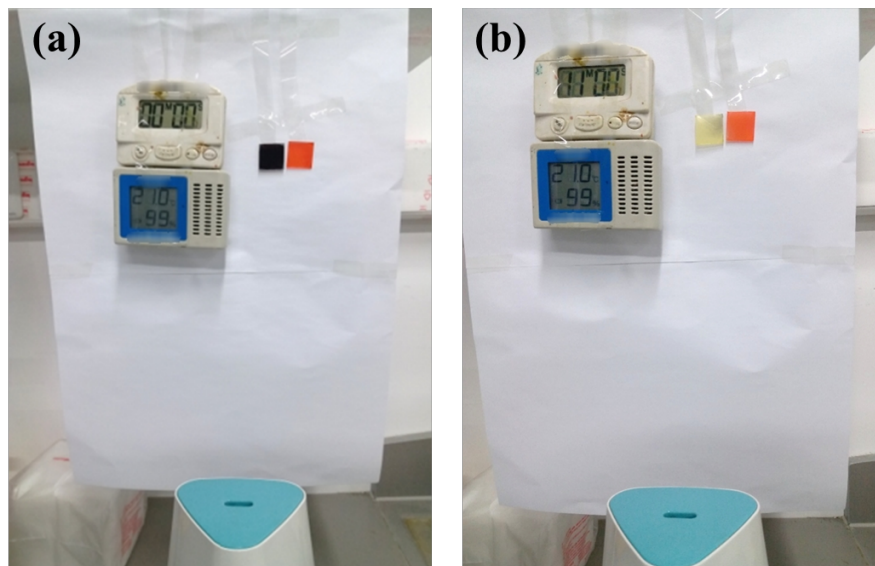


Figure S8. Photograph of the (a) initial and (b) final appearance of  $(3\text{-APN})_2\text{PbI}_4$  (right, orange color unchanged) and  $\text{CH}_3\text{NH}_3\text{PbI}_3$  (left, black color changed to white) films stored in a humidifier with the humidity of 99%.